NJC

Accepted Manuscript

This is an *Accepted Manuscript*, which has been through the Royal Society of Chemistry peer review process and has been accepted for publication.

Accepted Manuscripts are published online shortly after acceptance, before technical editing, formatting and proof reading. Using this free service, authors can make their results available to the community, in citable form, before we publish the edited article. We will replace this *Accepted Manuscript* with the edited and formatted *Advance Article* as soon as it is available.

You can find more information about *Accepted Manuscripts* in the Information for Authors.

Please note that technical editing may introduce minor changes to the text and/or graphics, which may alter content. The journal's standard Terms & Conditions and the Ethical guidelines still apply. In no event shall the Royal Society of Chemistry be held responsible for any errors or omissions in this *Accepted Manuscript* or any consequences arising from the use of any information it contains.

ROYAL SOCIETY OF CHEMISTRY

www.rsc.org/njc

Biocompatible Phosphate Anchored Fe_3O_4 Nanocarriers for Drug Delivery and Hyperthermia

Priyanka Sharma[a,b,‡], Suman Rana[a,‡], Kanhu C. Barick[a,*], Chandan Kumar[c], Hemant G. Salunke[d] and Puthussericka A. Hassan[a,*]

[a]*Chemistry Division, Bhabha Atomic Research Centre, Mumbai – 400 085, India*

[b]*Centre for Converging Technologies, University of Rajasthan, Jaipur – 302 004, India*

[c]*Isotope Production and Applications Division, Bhabha Atomic Research Centre, Mumbai – 400 085, India*

[d]*Technical Physics Division, Bhabha Atomic Research Centre, Mumbai-400085, India*

[*]*Corresponding authors:- Tel.: + 91 22 2559 0284, Fax:+ 91 22 2550 5051,*

Email: kcbarick@barc.gov.in (K. C. Barick), hassan@barc.gov.in (P. A. Hassan)

[‡]*These authors contributed equally to this work.*

Graphical Abstract

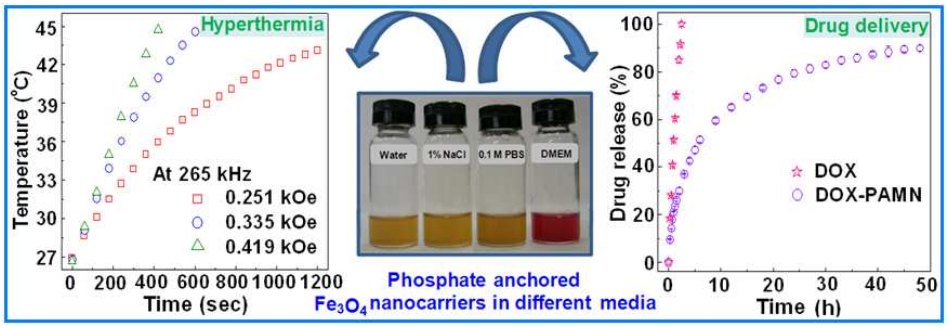

Development of water-dispersible phosphate anchored Fe_3O_4 magnetic nanocarriers by conjugation of bioactive sodium hexametaphosphate for drug delivery and hyperthermia applications.

New Journal of Chemistry Accepted Manuscript

Biocompatible Phosphate Anchored Fe_3O_4 Nanocarriers for Drug Delivery and Hyperthermia †

Priyanka Sharma[a,b,‡], Suman Rana[a,‡], Kanhu C. Barick[a,*], Chandan Kumar[c], Hemant G. Salunke[d] and Puthussericka A. Hassan[a,*]

[a]*Chemistry Division, Bhabha Atomic Research Centre, Mumbai – 400 085, India*

[b]*Centre for Converging Technologies, University of Rajasthan, Jaipur – 302004, India*

[c]*Isotope Production and Applications Division, Bhabha Atomic Research Centre, Mumbai – 400 085, India*

[d]*Technical Physics Division, Bhabha Atomic Research Centre, Mumbai-400085, India*

[*]*Corresponding authors:- Tel.: + 91 22 2559 0284, Fax:+ 91 22 2550 5051,*
Email: kcbarick@barc.gov.in (K. C. Barick), hassan@barc.gov.in (P. A. Hassan)

Abstract

We demonstrate the preparation of biocompatible, water-dispersible phosphate anchored Fe_3O_4 magnetic nanocarriers (PAMN) by a facile soft-chemical approach. The surface functionalization of Fe_3O_4 nanoparticles (~10 nm) with bioactive phosphate molecules (sodium hexametaphosphate) was evident from infrared, thermal and light scattering measurements. These superparamagnetic nanoparticles show better aqueous colloidal stability, good magnetic response and excellent self-heating efficacy under external AC magnetic field. The bioactive shell not only provides colloidal stability to the particles but also create functionalized exteriors with high densities of phosphate moieties for conjugation of drug molecules. The drug loading and release behavior of PAMN were investigated using doxorubicin hydrochloride (DOX) as a model drug to evaluate their potential as a carrier system. The cell viability and hemolysis assay suggest that PAMN do not have adverse toxic effects for further *in-vivo* use. Specifically, high loading affinity for DOX with their sustained release profile and self-heating capacity makes these novel nanocarriers suitable for drug delivery and magnetic hyperthermia.

Keywords: *Fe_3O_4, phosphate functionalization, nanocarrier, drug delivery, hyperthermia*

New Journal of Chemistry Accepted Manuscript

1. Introduction

Superparamagnetic iron oxide (Fe_3O_4) nanoparticles have received a great deal of attention due to their potential biomedical applications such as heating source for hyperthermia treatment of cancer, carrier for drug delivery and contrast agent for magnetic resonance imaging (MRI).[1-6] Among these applications, development of magnetic nanocarriers for intracellular drug delivery and hyperthermia treatment of cancer has drawn remarkable attention due to their unique physio-chemical properties, less side effects, site-selective targeting and localized heating of cancer cells. These applications require the magnetic nanocarriers to be biocompatible, water-stable and of narrow size distribution.[6-9] Furthermore, for most of these biomedical applications, the first significant challenge is to avoid unwanted uptake of iron oxide nanoparticles by the reticulo-endothelial system (RES). The next one is to achieve selective targeting of the nanocarrier to the site of interest for *in-vivo* studies. A critical step in developing such molecular probes is to engineer the surface of nanoparticles with bioactive molecules having numerous free targeting ligands. Thus, there is a growing interest in developing biocompatible magnetic nanocarriers with suitable surface functionality for intracellular drug delivery and hyperthermia.

The most common strategies used for surface functionalization of magnetic nanocarriers comprise coating of bioactive organic and inorganic molecules onto the surface of nanoparticles.[10]. The presence of these bioactive layers on the surface not only stabilizes the iron oxide nanoparticles, but also provides accessible surface for conjugation of biomolecules and drugs. Although many molecules such as organic ligands, surfactants, polymers, dendrimers, silica and gold coating are widely used to stabilize Fe_3O_4 suspensions,[9-16] the literature on use of bioactive phosphonates and phosphates on nanoparticle surfaces is not much reported. The phosphonates and phosphates have a strong affinity towards transition metal oxide surfaces,

New Journal of Chemistry Accepted Manuscript

especially for those containing tantalum, aluminium, cerium and iron oxide.[17-25] For instance, Yee *et al.* reported the adsorption of alkanephosphonic acids on the surface of amorphous ferric oxide particles and proposed two possible bonding schemes for the phosphonate ions on Fe^{3+}, i.e., one O or two O atoms of the phosphonate group binding onto the surface.[18] Sahoo *et al.* reported the formation of strong P-O-Fe bonding on the surface of alkyl phosphonates and phosphate coated Fe_3O_4 nanoparticles.[20] Lamanna et al.[25] developed dendrons having phosphonate head groups and grafted them to the surface of iron oxide nanoparticles. These dendronized iron oxide nanoparticles were shown to have enhanced MRI contrast properties compared to polymer-coated iron oxides nanoparticles. Moreover, these functionalized phosphonate and phosphate seems to have an acceptable biocompatibility and thus, they can serve as potential alternatives to fatty acids as coating agents for metal oxide surface.[20,26] Recently, sodium hexametaphosphate (SHMP) a food additive, is widely used as a stabilizer for generation of various nanoparticles such as Au, $BaSO_4$, ZnCdS and $ZnS:Cu^{2+}$ etc.[27-30] The oral toxicity limit of SHMP is 3053 mg kg^{-1} and therefore, its use as a stabilizer in the generation of nanoparticles is safe. However, there is hardly any report on the use of SHMP as a stabilizer in preparation of aqueous-stable Fe_3O_4 nanoparticles.

Herein, we report the development of bioactive phosphate anchored Fe_3O_4 magnetic nanocarriers having good colloidal stability, magnetic responsivity and specific absorption rate. This interfacial modification of nanoparticles allows us to create functionalized exteriors with high densities of phosphate moieties for conjugation of drug molecules. Specifically, high loading affinity for doxorubicin with their sustained release profile, self-heating capacity and low toxicity makes these novel nanoparticles suitable for drug delivery as well as hyperthermia treatment of cancer.

New Journal of Chemistry Accepted Manuscript

2. Materials and methods

2.1. Materials

Ferrous chloride tetrahydrate ($FeCl_2.4H_2O$, ≥99%), ferric chloride hexahydrate ($FeCl_3.6H_2O$, ACS reagent, 97%), doxorubicin hydrochloride (DOX, 98%), 3-(4,5-dimethyl-2-thiazolyl)-2,5-diphenyl-2H-tetrazolium bromide (MTT, ≥97.5%) and sodium dodecyl sulfate (SDS, ≥99%) were procured from Sigma-Aldrich, USA. Acetic acid (AR grades) was purchased from Thomas Baker Chemical Pvt. Ltd., India. Sodium hexametaphosphate, sodium oxalate and sodium chloride, N,N-dimethylformamide (AR grades) were procured from S. D. Fine-chem Ltd., India. The acetate buffer (AB pH-5) and phosphate buffered saline (PBS-pH 7.3) were prepared using standard protocols.

2.2. Synthesis of phosphate anchored Fe_3O_4 magnetic nanocarriers

Fe_3O_4 magnetic nanoparticles were prepared by modified coprecipitation method.[31-33] In a typical synthesis of phosphate anchored Fe_3O_4 magnetic nanocarriers (PAMN), 5.406 g of $FeCl_3.6H_2O$ and 1.988 g of $FeCl_2.4H_2O$ were dissolved in 80 ml of Milli Q water in a round bottom flask and temperature was slowly increased to 70 ^oC in refluxing condition under nitrogen atmosphere with constant stirring. The temperature was maintained at 70 ^oC for 30 min and then 30 ml of 25% ammonia solution was added instantaneously to the reaction mixture, and kept for another 30 min at 70 ^oC. Then, 10 ml aqueous solution of excess SHMP (2 gm) was added and the temperature was slowly raised up to 90 ^oC under reflux and reacted for 60 min with continuous stirring for functionalization of Fe_3O_4 nanoparticles with phosphate molecules. The obtained black colored precipitates were then thoroughly rinsed with water and separated from the supernatant using a permanent magnet (field strength ~ 2.5 kOe).

New Journal of Chemistry Accepted Manuscript

2.3. Characterizations

X-ray diffraction (XRD) pattern was recorded on a Phillips PW1729 diffractometer with Cu Kα radiation. The crystallite size is estimated from the X-ray line broadening using Scherrer formula. The infrared spectra were recorded in the range 4000-400 cm^{-1} on a Fourier transform infrared spectrometer (FTIR, Bomem, MB series). The transmission electron micrographs were taken by Philips CM 200 TEM for particle size determination. Dynamic light scattering (DLS) measurements were performed using a Malvern 4800 Autosizer employing a 7132 digital correlator. The zeta-potential measurements were performed by Malvern Zetasizer nano series. The field (magnetic hysteresis) and temperature (zero field cooled-field cooled, ZFC-FC) dependent magnetization measurements were carried out by SQUID magnetometer. The colloidal stability was investigated by measuring the absorbance of PAMN suspensions (0.1 mg/ml) in different medium at a wavelength of 350 nm using JASCO V-650, UV-visible spectrophotometer. The concentrations of iron and phosphorus were measured by inductively coupled plasma-mass spectrometer (ICP-MS, VG PQ ExCell, VG Elemental).

The heating ability of PAMN was obtained from the time-dependent calorimetric measurements using an induction heating unit (Easy Heat 8310, Ambrell). 1 ml (1 mg/ml of Fe) aqueous suspension of PAMN was taken in a polypropylene sample holder with suitable arrangements to minimize the heat loss. The AC magnetic fields (AMF) of 0.251, 0.335 and 0.419 kOe at a fixed frequency of 265 kHz were used to evaluate the specific absorption rate (SAR). The SAR was calculated using the following equation:

$$SAR = C\frac{\Delta T}{\Delta t}\frac{1}{m_{Fe_3O_4}}$$

where, C is the specific heat of solvent ($C = C_{water} = 4.18$ J/g °C), $\Delta T/\Delta t$ is the initial slope of the time-dependent temperature curve and $m_{Fe_3O_4}$ is mass fraction of Fe_3O_4 in the sample.

New Journal of Chemistry Accepted Manuscript

The anticancer agent, doxorubicin hydrochloride (DOX) was used as a model drug to estimate the drug release behavior of the PAMN. In order to investigate the interaction of drug molecules with PAMN, we have studied the fluorescence spectra of pure DOX and DOX loaded PAMN in addition to zeta-potential measurements. The aqueous dispersion of different amounts of PAMN (0, 20, 40, 60, 80, 100, 120 and 140 μg from a stock suspension of 2 mg/ml) were added to a 1 ml of DOX solution (10 μg/ml) and mixed thoroughly by shaking at room temperature for 15 min. The fluorescence spectra of the supernatant (obtained after magnetic sedimentation of drug loaded PAMN) were then recorded using Hitachi F4500 fluorescence spectrophotometer. The fluorescence intensities of supernatants (washed drug molecules were also taken into consideration for calculations) against that of pure DOX solution were used to determine the loading efficiency (binding isotherm). The loading efficiency (w/w %) was calculated using the following relation:

$$\text{Loading efficiency } (\%) = \frac{(I_{DOX} - I_S - I_W)}{I_{DOX}} \times 100$$

where, I_{DOX} is the fluorescence intensity of pure DOX solution, I_S the fluorescence intensity of supernatant and I_W the fluorescence intensity of washed DOX (physically adsorbed DOX molecules).

For release study, we have quantified the amount of DOX loaded PAMN according to the binding isotherm. The loading was carried out, at increased scale, by incubating 0.5 ml of aqueous solution of DOX (1 mg/ml) with 2.5 ml of the aqueous suspension of PAMN (5 mg) for 1h in the dark (however, no decrease in fluorescence intensities was observed after 15 min of incubation). The pH triggered drug release studies were carried out under reservoir (r) - sink (s) conditions (AB-pH 5 vs. AB-pH-5, AB-pH 5 vs. PBS pH-7.3, PBS-pH 7.3 vs. PBS-pH 7.3). The drug-loaded PAMN (5 mg) were immersed in 5 ml of pH 5/pH 7.3 and then added into a dialysis

New Journal of Chemistry Accepted Manuscript

bag. The dialysis was performed against 200 ml of the respective-sink medium under continuous stirring at 37 °C to mimic the cellular environment. One ml of the external medium was withdrawn and replaced with the same fresh medium at fixed intervals of time to maintain the sink conditions. The amount of DOX released was determined by measuring the fluorescence emission at 585 nm (excitation wavelength: 490 nm) using a plate reader (Infinite M1000, Tecan-I control) against the standard plot prepared under similar conditions. Each experiment was performed in triplicates and the standard deviation was given in the plot. Further, drug release studies were carried out under sink condition in presence and absence of AMF. The AB-pH 5/ PBS-pH 7.3 dispersions of DOX loaded PAMN (taken in a polypropylene sample holder) was placed under AMF. The AMF of 0.335 kOe was applied to attain 42-43 °C (hyperthermia temperature) and this temperature was maintained for another 10 min by varying the AMF. The particles were separated by using permanent magnet and the supernatant was used for determination of DOX released as mentioned above. The controlled experiments were carried out under similar conditions without using AMF.

The biocompatibility of the PAMN with MG63 (Osteosarcoma) cells were evaluated using the MTT assay. MG63 cells were obtained from the National Center for Cell Sciences (NCCS), Pune, India and routinely cultured in MEM (Sigma Inc. MO, USA) supplemented with 10 % serum (Invitrogen CA, USA) and antibiotic solution. For biocompatibility study, the cells were first seeded into a 96-well plate at densities of 1×10^3 cells per well for 24 h. Then different concentrations of PAMN suspension (0, 1.2, 9.65, 33.45, 50, 100 and 250 µg/ml) were added to each wells and incubated for another 24 h in 5 % CO_2 at 37 ^oC. The cells supernatant was discarded and thereafter, 10 µl of MTT solution (5 mg/ml) was added and incubated for 4 h. Formazan crystal was solubilized by addition of 200 µl of solubilizing buffer (20 % SDS in 50 %

New Journal of Chemistry Accepted Manuscript

DMF). The 96-well plate was centrifuged at 2000 rpm for 5 min and kept on magnetic rack for an hour. Supernatant was transferred into a new 96-well plate and absorbance was measured at 570 nm with reference to 630 nm in BioTek Universal Microplate Reader (BioTek Inc. USA). The percentage of cell proliferation was calculated as ratio of optical density (OD) of treated and control cells multiplied by 100. Further, the cytotoxicity of pure DOX and DOX-PAMN (0.125 and 1 μM DOX) were also evaluated using the MTT assay. The drug concentrations were chosen based on the 50% inhibitory concentration (IC50) value of DOX for MG63 cells (Fig. S1, ESI). For IC50 value of DOX, 1×10^3 cells were incubated with different amount of DOX (0.015-5μM) for 24 h and then processed for MTT assay.

In order to determine the hemocompatibility of PAMN, hemolysis ratio (HR) was measured. Briefly, 5 ml human blood was mixed with 2 ml sodium oxalate (2 wt. %) and 2.5 ml solution of sodium chloride (NaCl, 0.9 wt. %). Next, 2 mg of PAMN was added to 10 ml of 0.9 wt. % NaCl solution and incubated at 37 ^{o}C for 30 min. Subsequently, 0.2 ml diluted blood was added into the prepared samples and incubated at 37 ^{o}C for another 30 min. The liquid was centrifuged at 3000 rpm for 5 min. The absorbance of the supernatant (hemoglobin concentration) was measured with a UV-visible spectrophotometer at wavelength of 545 nm. The negative (in 0.9 wt. % NaCl solution) and the positive control (in Milli Q water) were also prepared. The percentage of hemolysis was calculated as follows:

$$\text{Hemolysis } (\%) = \frac{A_s - A_{neg}}{A_{pos} - A_{neg}} \times 100$$

where, A_s, A_{neg}, A_{pos} are the absorbance of the sample, the negative control and the positive control, respectively. The percentage of hemolysis was calculated based on the average of three replicates. High hemocompatibility was given for samples with < 5% hemolysis,

New Journal of Chemistry Accepted Manuscript

hemocompatible for samples within 10% hemolysis, and non-hemocompatible for > 20% hemolysis.

The detection of protein corona (protein-particle interaction) formed around the nanoparticle from either plasma or cytosolic fluids was carried out according to the protocol by Lundqvist et al.[34] Briefly, nanoparticle in 10 mM phosphate buffer pH-7.5, 0.15M NaCl and 1mM EDTA were incubated with either plasma (200 µl) or cytosolic fluids (500 µl) for an hour (isolation procedures of plasma and cytosolic fluids are provided in supplementary information, ESI†). Samples were centrifuged at 16000 ×g for 5 min and washed thrice with 1 ml of 10 mM PBS pH-7.5, 0.15 M NaCl and 1 mM EDTA. Nanoparticle bound protein was mixed with 2×SDS-PAGE loading buffer and loaded onto 12% SDS-PAGE gel to resolve the different proteins. The protein containing SDS-PAGE gel was stain in 0.25% staining solution (0.25g of Coomassie Brilliant blue R250 in 50 ml of methanol, 40 ml of water and 10 ml of acetic acid) on slowly rocking platform for 4 h at room temperature to visualize the protein bands. Destaining of gel was done with destaining solution (50 ml of methanol, 40 ml of water and 10 ml of acetic acid) on a slowly rotating platform for 24h with slight heating. Gel photograph was taken in high resolution scanner.

3. Results and discussion

PAMN were prepared by *in-situ* functionalization of Fe_3O_4 nanoparticles with SHMP during co-precipitation of Fe^{2+} and Fe^{3+} ions in basic medium. SHMP was chosen as the coating material due to its low toxicity and immunogenicity. Fig. 1 shows (a) XRD pattern and (b) TEM micrograph of PAMN. The XRD pattern reveals the formation of single-phase Fe_3O_4 inverse spinel structure with lattice constant, a = 8.377 Å, which is very close to the reported value of magnetite (JCPDS Card No. 88-0315, a = 8.375 Å). The presence of sharp and intense

New Journal of Chemistry Accepted Manuscript

diffraction peaks confirmed the formation of highly crystalline nanoparticles. The average crystallite size of nanoparticles is found to be around 10 nm from X-ray line broadening using the Scherrer formula. TEM micrograph of PAMN clearly shows the formation of roughly spherical Fe_3O_4 nanoparticles of size about 10 nm. The selected area electron diffraction pattern (inset of Fig. 1b) also confirmed the high crystallinity of PAMN. It can be indexed to highly crystalline reflections, such as (220), (311), (400), (422), (511) and (440) of cubic inverse spinel Fe_3O_4 structure, which is consistent with the XRD result.

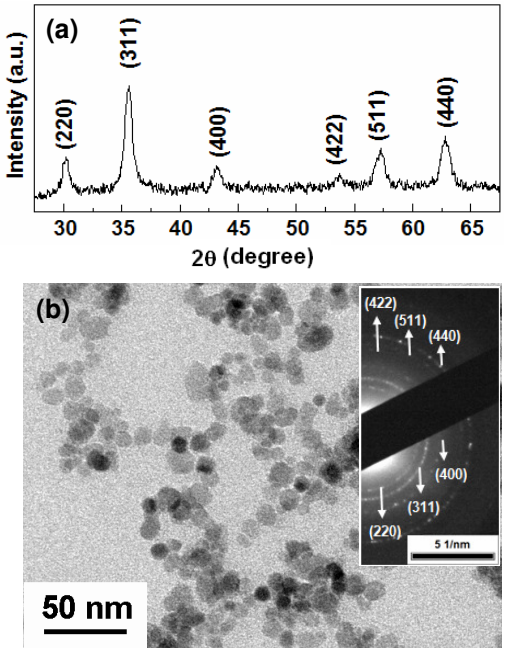

Fig. 1. (a) XRD pattern and (b) TEM micrograph of PAMN (inset of Fig. 1b shows its selected area electron diffraction pattern).

Fig. 2 shows the FTIR spectra of SHMP and PAMN along with their peak assignments. The IR bands for the pure SHMP are well resolved, but those of the PAMN are rather broad and a few. The strong IR band observed at around 577 cm^{-1} in PAMN can be ascribed to the Fe-O stretching vibrational mode of Fe_3O_4. The broad IR spectrum observed in the range of 800 to 1220 cm^{-1} with band at 915, 1030, 1090 and 1175 cm^{-1} in PAMN can be assigned to $P\text{-}O^-$

New Journal of Chemistry Accepted Manuscript

vibrations of SHMP.[35,36] Further, the IR bands observed at around 1400 cm^{-1} and shoulder at 710 cm^{-1} can be associated with P=O and P-O-P stretching vibrations, respectively.[36] These results clearly suggested the successful anchoring/grafting of phosphate groups of SHMP onto the surface of Fe_3O_4 nanoparticles. The bending and stretching vibrational modes of absorbed H_2O molecules are appeared at 1630 and 3400 cm^{-1}, respectively. Further, TGA analysis (Fig. S2, ESI) also confirmed the presence of organic molecules on the surface of Fe_3O_4 nanoparticles. From ICP-MS analysis, it has been found that only 5% of the used SHMP molecules were coated onto the surface of Fe_3O_4 nanoparticles under the present experimental conditions. However, we have removed all free SHMP present in the solution by magnetic separation followed by through washing.

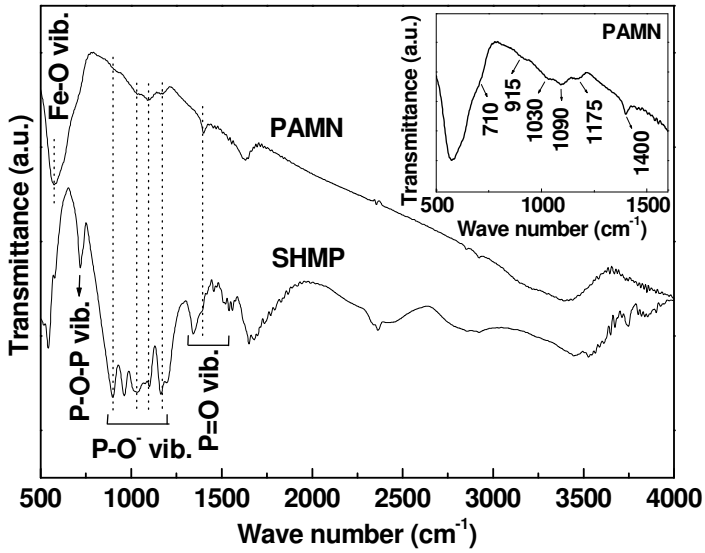

Fig. 2. FTIR spectra of SHMP and PAMN along with their peaks assignment (inset shows the expanded FTIR spectrum of PAMN in the range of 500 – 1600 cm^{-1}).

Fig. 3 shows the zeta-potential (ζ) measurements of PAMN at different pH. The surface of PAMN shows negatively charged and pH of zero point charge was not observed in the

New Journal of Chemistry Accepted Manuscript

measured pH range. However, the negative surface charge decreases with decrease in pH of the medium. This variation in surface charge may be attributed to the degree of ionization of functional groups (phosphate moieties) associated with Fe_3O_4 nanoparticles at different pH. DLS measurement (inset of Fig. 3) indicates that these samples render aqueous colloidal suspension with intensity weighted (z-average) hydrodynamic diameter of about 100 nm due to the presence of associated and hydrated organic layers.[6,37] The observed higher hydrodynamic diameter could also arise from the polydispersity of the nanoparticles. As DLS is weighted towards large sizes, the average diameter could be higher than those obtained from TEM. However, the average hydrodynamic diameter hardly varies with time revealing their good aqueous colloidal stability (inset of Fig. 3). The structure of SHMP consists of six phosphate anions, which are linked to each other to form a ring-like structure, with each phosphate group linked to one sodium atom outside the ring. Specifically, some of the phosphate groups of SHMP strongly coordinate to iron cations on the Fe_3O_4 surface to form a robust coating, while the remaining functionalized exteriors of PAMN extend into the water medium, conferring a high degree of aqueous colloidal stability to Fe_3O_4 nanoparticles. In addition to this, the electrostatic repulsive force originating from the ionization of the surface groups also provide stability to the nanoparticles. Furthermore, the highly negative values of zeta-potential of PAMN in 1 % NaCl (ζ = -20 mV) and 0.01 M PBS, pH 7.3 (ζ = -25 mV) indicate their excellent stability in physiological medium. The colloidal stability of the PAMN was also assessed from the changes in absorbance of PAMN suspensions. The insignificant change in absorbance of PAMN suspension (0.1 mg/ml) in aqueous and cell culture (DMEM + 10% FBS) media with time indicates their good colloidal stability (Fig. S3, ESI).

New Journal of Chemistry Accepted Manuscript

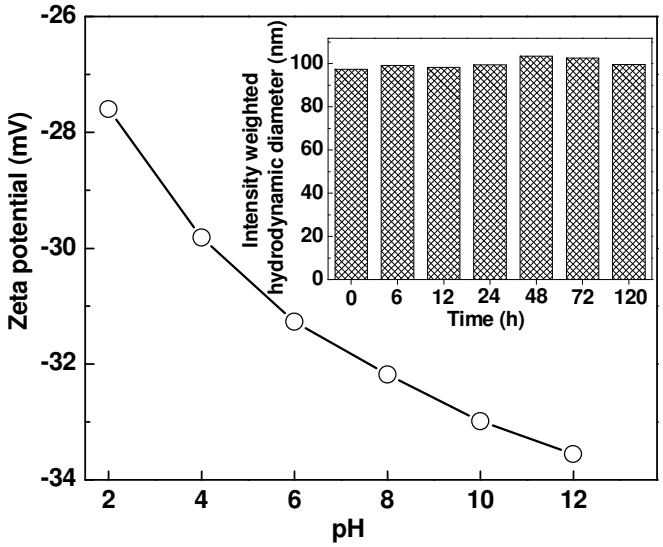

Fig. 3. Zeta-potential (ζ) measurements of PAMN at different pH (inset shows the variation of intensity weighted (z-average) hydrodynamic diameter of PAMN as a function of time).

In order to assess the potential of PAMN in targeted drug delivery and hyperthermia, we have investigated their magnetic field responsivity and heating efficacy under AC magnetic field. Fig. 4 shows the field dependent magnetization (M vs. H) plots of PAMN at 5 and 280 K. At 280 K, PAMN exhibit superparamagnetic behavior without coercivity (H_C) and remanence magnetization (R_m), whereas ferrimagnetic behavior with H_C = 200 Oe and R_m = 14 emu/g is observed at 5 K. The appearance of hysteresis loop at 5 K suggests magnetic ordering in sample at the lower temperature. This transition from superparamagnetic behavior at high temperature to ferro or ferrimagnetic behavior below the so-called blocking temperature is typically observed in MNPs.[12] The ZFC-FC plots (top inset of Fig. 4) shows that the blocking temperature (T_B) of the PAMN is 105 K at an applied field of 400 Oe. However, T_B is found to decrease with the increase of applied field (Fig. S4, ESI). The superparamagnetic blocking process is the competition between thermal and anisotropy energies of the particles. At higher applied field, the anisotropy energy of the particles decreases and less thermal energy is required to overcome the

New Journal of Chemistry Accepted Manuscript

energy barrier and thus the blocking temperature decreases.[38] The maximum magnetizations (at an applied field of 6 kOe) of PAMN were found to be 47.8 and 55 emu/g at 280 and 5 K, respectively. It has been observed that the room temperature magnetization of PAMN was reduced to about 52 % of the bulk Fe_3O_4 (92 emu/g). This decrease in magnetization can be attributed to the combined effect of nano size of core Fe_3O_4 particles (large surface to volume ratio) and robust coating of SHMP molecules on their surface. However, the retention of superparamagnetic property at room temperature with good magnetic field responsivity (bottom inset of Fig. 4) makes these nanoparticles suitable for drug delivery and hyperthermia applications.

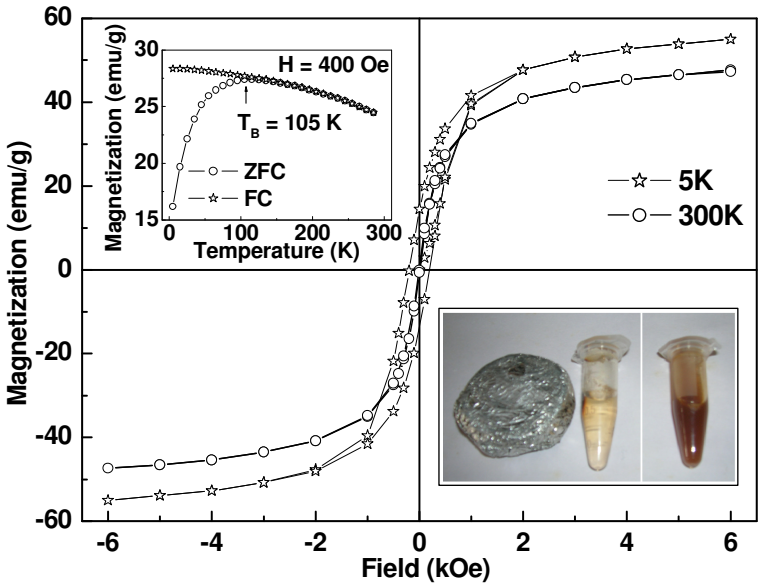

Fig. 4. (a) Field M vs. H plots of PAMN at 5 and 300 K and (top inset shows their ZFC-FC plot at an applied field of 400 Oe and bottom inset shows the magnetic responsiveness of PAMN suspension in presence and absence of magnetic field).

The temperature *vs.* time plots of PAMN suspension showed a time-dependent gradual increase in temperature under AC magnetic fields (Fig. 5). It has been observed that a magnetic field of 0.251 kOe at fixed frequency of 265 kHz is able to produce energy enough for raising the

New Journal of Chemistry Accepted Manuscript

temperature of the magnetic suspension of 1 mg/ml to 42-43 ^{o}C within 20 min. Further, the time required to reach 43 °C decreases with an increase in field strength, which is obvious as the heat generation/dissipation (*P*) is proportional to the square of applied AC magnetic field (inset of Fig. 4b) as follows[39,40]:

$$P = \pi\mu_0\chi_0 H^2 f \frac{2\pi f\tau_{eff}}{1+(2\pi f\tau_{eff})^2}$$

where μ_0 is the permeability of free space, χ_0 is the magnetic susceptibility, *H* is the magnetic field amplitude and τ_{eff} is the effective relaxation time. In order to elucidate that the rise in temperature is mainly due to the presence of PAMN under AMF but not from applied AMF alone, we have carried out control experiments, where water solution (without PAMN) were exposed to AMF under similar conditions. It has been observed that AMF alone was not significantly heating water (temperature was raised only to 29.7 and 32.8 ^{o}C even after 20 min exposure of AMF of 0.251 and 0.335 kOe, respectively, Fig. S5, ESI).

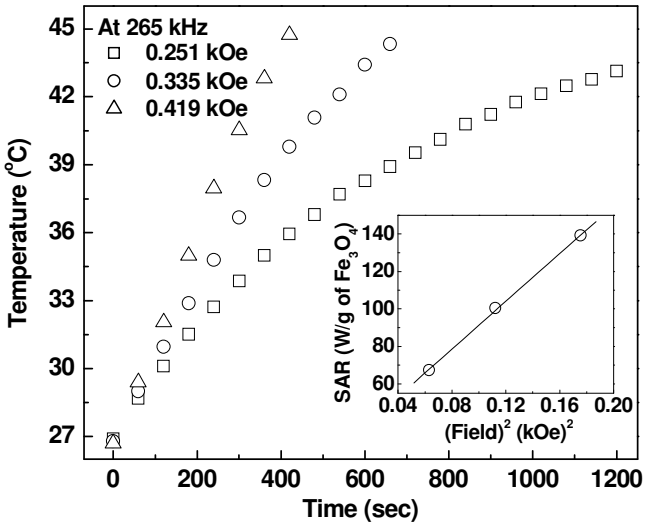

Fig. 5. Temperature vs. time plots of 1 ml aqueous suspension of PAMN (1 mg/ml of Fe) at different applied field (inset shows the linear relationship between SAR and square of the applied AC magnetic field).

New Journal of Chemistry Accepted Manuscript

In thermal activation of Fe_3O_4 nanoparticles under AC magnetic field, an increase in temperature is mainly due to the combined effect of Néel and Brownian relaxations.[40-42] The Néel relaxation is associated with the magnetic moment rotations within the particles due to internal fluctuations of the magnetic moment with respect to the crystal lattice. The Brownian relaxation is related to the rotation of entire particles due to mechanical friction with the surrounding medium when nanoparticles keep oscillating towards the field, keeping its magnetic moment fixed along the crystal axis. The relaxation times are given by the following equations[39,40]:

$$\tau_N = \tau_0 e^{KV_M/k_BT}$$

$$\tau_B = \frac{4\pi\eta R_H^{\ 3}}{k_BT}$$

$$\tau_{eff} = \frac{\tau_N \tau_B}{\tau_N + \tau_B}$$

where τ_B is the Brownian relaxation time, τ_N is the Néel relaxation time, $\tau_0 \approx 10^{-9}$s, K is the anisotropy constant, V_M is the volume of the Fe_3O_4 nanoparticle, k_B is Boltzmann's constant, T is temperature, η is the viscosity and R_H is the hydrodynamic particle radius. The use of magnetic nanoparticles in hyperthermia therapy depends on their heating efficiency, which is expressed in terms of the specific absorption rate (SAR). The SAR values of PAMN were found to be 67.3, 100.5 and 139.2 W/g of Fe_3O_4 with an applied field of 0.251, 0.335 and 0.419 kOe, respectively. The observed good SAR is likely to be due to a combination of their good magnetic responsivity and aqueous colloidal stability. However, SAR is dependent on various parameters such as concentration of particles, magnitude of frequency and physical properties of magnetic particles (magnetization, particles size, size distribution and hydrodynamic radius of particles).[7,43] Thus,

New Journal of Chemistry Accepted Manuscript

the observed SAR values should not be viewed in terms of performances, but only as a demonstration that these nanocarriers are effective heating source for hyperthermia treatment of cancer.

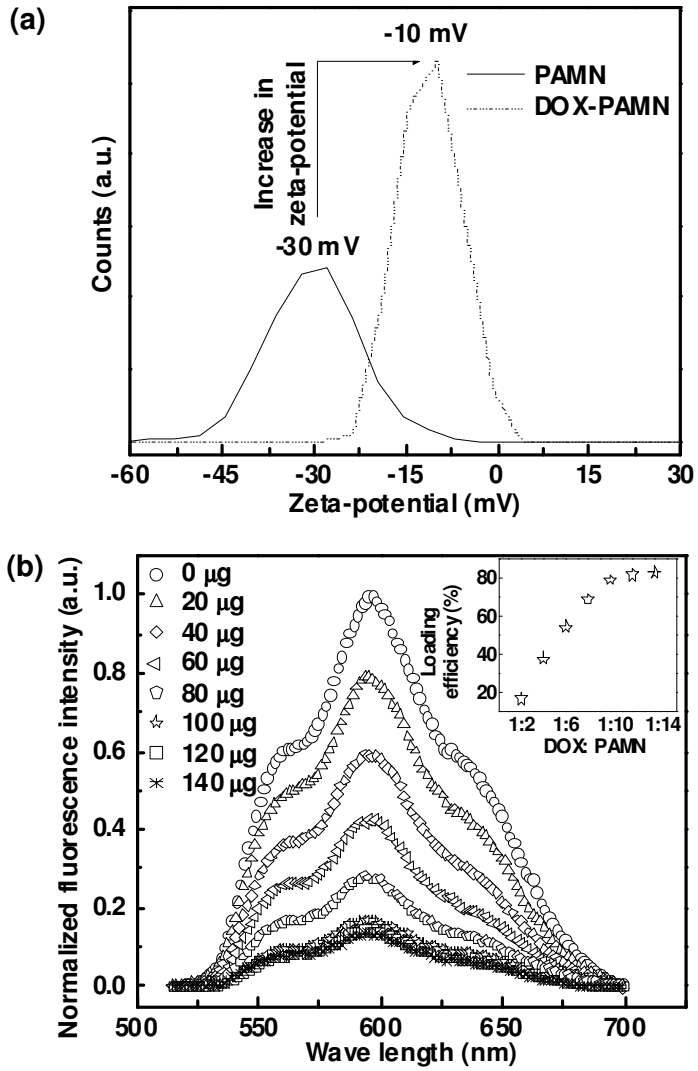

Fig. 6. (a) Zeta-potential of 1 ml aqueous suspension of PAMN (100 µg/ml) before and after interaction with 10 µg/ml of DOX and (b) fluorescence spectra of 1 ml aqueous solution of pure DOX (10 µg/ml) before and after interaction with different amount of PAMN (inset of Fig. 6b shows the loading efficiency of DOX onto PAMN after considering the washed drug molecules for calculations).

New Journal of Chemistry Accepted Manuscript

Fig. 6 shows the (a) zeta-potential of 1 ml aqueous suspension of PAMN (100 µg/ml) before and after interaction with 10 µg/ml of DOX and (b) fluorescence spectra of 1 ml aqueous solution of pure DOX (10 µg/ml) before and after interaction with different amount of PAMN. The zeta-potential of PAMN suspension (100 µg/ml) increased from -30 mV to -10 mV upon incubating with an aqueous solution of 10 µg/ml of DOX. This increase in zeta-potential arises from the binding of cationic DOX (protonated primary amine present on DOX induces a positive charge) with negatively charged PAMN by forming DOX-PAMN system predominately through electrostatic interactions. The affinity of DOX for negatively charged molecules such as carboxylate ions and phospholipids has been subject of numerous earlier investigations.[3,16,44,45] The interaction of DOX molecules with PAMN was also evident from the decrease in fluorescence intensity of the supernatant liquid after removal of DOX bound PAMN through magnetic separation (Fig. 6b). Furthermore, the fluorescence intensity of supernatant liquid decreases with increasing the concentration of PAMN, which is obvious due to the increase in loading efficiency of DOX onto the surface of PAMN. It has been observed that the loading efficiency (inset of Fig. 6b) is strongly dependent on the weight ratio of PAMN to DOX and a drug loading efficiency (w/w) of about 82% is achieved at PAMN to DOX weight ratio of 14 (no significant increase in loading efficiency is observed above this ratio). It is worth mentioning that PAMN still preserve good dispersibility after being coupled with DOX molecules (variation of intensity average diameter of DOX loaded PAMN as a function of time, Fig. S6, ESI).

New Journal of Chemistry Accepted Manuscript

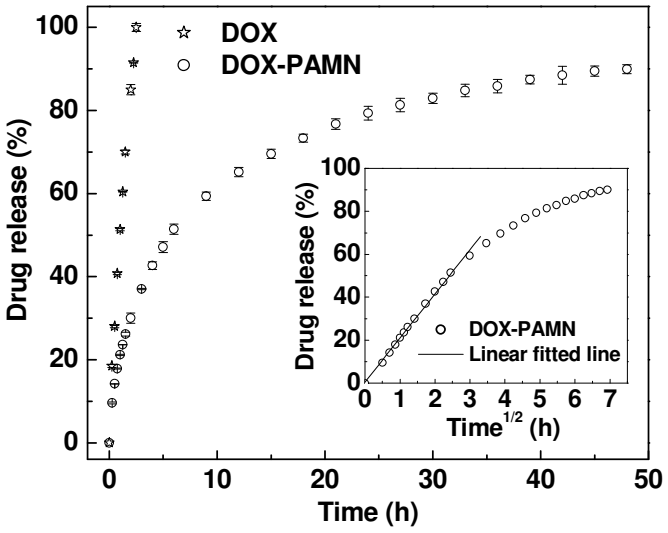

Fig. 7. Drug release profile of pure DOX and DOX-PAMN in cell mimicking environment (reservoir: pH 5 and sink: pH 7.3) at 37 °C.

Drug release profiles of pure DOX and DOX loaded PAMN were investigated under reservoir-sink condition (reservoir: pH 5 and sink: pH 7.3) at a temperature of 37 °C. The release of drug molecules from DOX-PAMN (Fig. 7) follows a time dependent release profile. While pure DOX shows the rapid release behavior with $t_{1/2}$ (time needed for the release of 50% of the dose) about 45 min, the DOX-PAMN show sustained release profile with $t_{1/2}$ about 6 h. It has been observed that about 90% of loaded drug molecules were released from the DOX-PAMN system at pH 5. Furthermore, the short time release behavior of DOX from DOX-PAMN (inset of Fig. 7) shows a linear relationship between the drug release and square root of time ($t^{1/2}$) as expected from Higuchi drug release model confirming that the DOX release process is diffusion-controlled.[46] We have also carried out the drug release studies by keeping same pH for reservoir and sink (pH 5 vs. pH 5 and pH 7.3 vs. pH 7.3, Fig. S7, ESI) to estimate more precisely the contribution of the pH gradient on the DOX release from the DOX-PAMN system. Our release studies indicate triggered release of electrostatically bound drug molecules at acidic environment

New Journal of Chemistry Accepted Manuscript

(percentage of drug release is much higher at pH 5 vs. pH 5 and pH 5 vs. pH 7.3 than pH 7.3 vs. pH 7.3). This is desirable for cancer therapy as the relatively low pH in tumors will specifically stimulate the release of drug at the target site. The pH triggered release of DOX could be attributed to the weakening of the electrostatic interactions between the drug and the partially neutralized phosphate groups on the nanocarrier surface. Further, drug release studies were carried out in pH 7.3 and pH 5 under AMF in sink condition. There is no significant release of drug was observed under AMF as compared to their respective control experiments (Fig. S8, ESI). Recently, Oliveira et al.[47] reported magnetic field triggered drug release from hybrid polymersomes (loaded with DOX and iron oxide nanoparticles). They have observed significant increase in drug release by exposing hybrid polymersomes to magnetic field and hypothesized that a local heating leads to a permeation of the polymersome membrane facilitating DOX release. However, in present case local heating is not capable of release electrostatically bound drug from the nanocarriers.

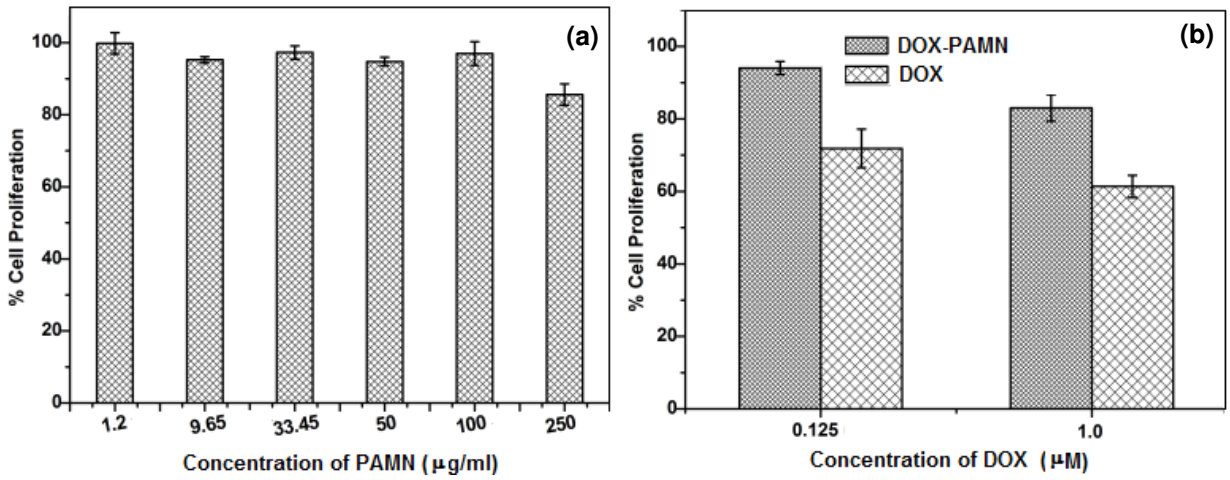

Fig. 8. Viabilities of MG63 cells incubated in medium containing difference concentrations of (a) PAMN and (b) DOX and DOX-PAMN at 37 ^{o}C for 24 h.

New Journal of Chemistry Accepted Manuscript

Biomedical application of nanoparticles involves their intentional exposure to the human body. Therefore, understanding the properties of nanoparticles and their effects on the human body is crucial before they are applied clinically. Our MTT assay showed that more than 85% of MG63 cells were viable, even after 24 h incubation with 250 μg/ml of PAMN (Fig. 8a). This result suggests that these phosphate functionalized nanoparticles are biocompatible and do not have toxic effect for further *in-vivo* use. However, DOX and DOX-PAMN show toxicity to the proliferation of MG63 cells (Fig. 8b). The relatively lower cytotoxicity of DOX-loaded PAMN, compared to DOX, can be attributed to the sustained release behavior of the nanocarriers (loaded drug is expected to release slowly over the experimental period). Furthermore, the percentage of hemolysis was found to be around 2.5% upon incubation of 0.5 mg of PAMN, which indicates their good hemocompatibility. However, our SDS-PAGE staining studies (Fig. S9, ESI) with Coomassie Brilliant blue R250 showed the various protein bands ranging from 205 kDa to 6.5 kDa, in both plasma and cytosolic fluid incubated nanoparticles. This result indicates the interaction of nanoparticles with proteins of plasma and cytosolic fluid. The dynamic layer of proteins, so called protein corona on the PAMN surface determines its ability to interact with the living system and thereby modifies the cellular uptake/response of these nanoparticles. Thus, further studies are required to evaluate the importance of protein-particle interaction in nanotoxicity and prevention of opsonization in biological environment. Specifically, present study demonstrates the preparation of highly crystalline, water dispersible, bioactive phosphate anchored Fe_3O_4 magnetic nanocarriers having excellent self-heating efficacy and their applications in drug delivery and hyperthermia.

New Journal of Chemistry Accepted Manuscript

4. Conclusion

A simple facile approach for the synthesis of phosphate anchored Fe_3O_4 aqueous colloidal magnetic nanocarriers of average size about 10 nm is demonstrated. XRD and TEM analysis confirmed the formation of highly crystalline single phase Fe_3O_4 nanostructures. The detailed structural analyses by FTIR, TGA, DLS and zeta-potential confirmed the successful functionalization of Fe_3O_4 nanoparticles with phosphate molecules. These superparamagnetic nanocarriers exhibit better colloidal stability and good biocompatibility with excellent heating efficacy under AC magnetic field. Furthermore, nanoparticles showed high loading affinity for DOX and their sustained release profile under acidic environment. This sustained release of drug is desirable for cancer therapy as the relatively low pH in tumors will specifically stimulate the release of drug at the target site. The high loading affinity for DOX with their sustained release profile and self-heating capacity, makes these nanocarriers suitable for drug delivery as well as hyperthermia treatment of cancer. Specifically, this study demonstrates a tailored approach for generating novel biocompatible magnetic probes for clinical applications.

Acknowledgment

The authors acknowledge Prof. D. Bahadur, Indian Institute of Technology Bombay, Mumbai, India for his encouragement and allowing us to use some of the experimental facilities. The authors also thank Dr. R. S. Ningthoujam, Bhabha Atomic Research Centre, Mumbai, India for facilitating the use of induction heater.

† **Electronic Supplementary Information (ESI) available.** The isolation procedures of plasma and cytosolic fluids and Fig. S1-S9.

‡ **These authors contributed equally to this work.**

New Journal of Chemistry Accepted Manuscript

References

1. S. Mornet, S. Vasseur, F. Grasset and E. Duguet, *J. Mater. Chem.*, 2004, **14**, 2161.
2. P. B. Shete, R. M. Patil, R. S. Ningthoujam, S. J. Ghosh and S. H. Pawar, *New J. Chem.*, 2013, **37**, 3784.
3. S. Nigam, K. C. Barick and D. Bahadur, *J. Magn. Magn. Mater.*, 2011, **323**, 237.
4. S. Li, Y. Ma, X. Yue, Z. Cao and Z. Dai, *New J. Chem.*, 2009, **33**, 2414.
5. J. -H. Lee, Y. -M. Huh, Y. Jun, J. -W. Seo, J. -T. Jang, H. -T. Song, S. J. Kim, E. -J. Cho, H. -G. Yoon, J. -S. Suh and J. Cheon, *Nat. Med.*, 2007, **13**, 95.
6. K. C. Barick, M. Aslam, Y. P. Lin, D. Bahadur, P. V. Prasad and V. P. Dravid, *J. Mater. Chem.*, 2009, **19**, 7023.
7. B. Samanta, H. Yan, N. O. Fischer, J. Shi, D. J. Jerry and V. M. Rotello, *J. Mater. Chem.*, 2008, **18**, 1204.
8. A. Tomitaka, T. Koshi, S. Hatsugai, T. Yamada and Y. Takemura, *J. Magn. Magn. Mater.*, 2011, **323**, 1398.
9. K. C. Barick, S. Singh, D. Bahadur, M. A. Lawande, D. P. Patkar and P.A. Hassan, *J. Coll. Interf. Sci.*, 2014, **418**, 120.
10. S. Laurent, D. Forge, M. Port, A. Roch, C. Robic, L. V. Elst and R. N. Muller, *Chem. Rev.*, 2008, **108**, 2064.
11. S. Mondini, S. Cenedese, G. Marinoni, G. Molteni, N. Santo, C. L. Bianchi and A. Ponti, *J. Coll. Interf. Sci.*, 2008, **322**, 173.
12. K. C. Barick and P. A. Hassan, *J. Coll. Interf. Sci.*, 2012, **369**, 96.
13. S. C. Wuang, K. G. Neoh, E. -T. Kang, D. W. Pack and D. E. Leckband, *J. Mater. Chem.*, 2007, **17**, 3354.

New Journal of Chemistry Accepted Manuscript

14. B. González, E. Ruiz-Hernández, M. J. Feito, C. L. Laorden, D. Arcos, C. Ramírez-Santillán, C. Matesanz, M. T. Portolés and M. Vallet-Regí, *J. Mater. Chem.*, 2011, **21**, 4598.

15. H. H. P. Yiu, H. -J. Niu, E. Biermans, G. Tendeloo and M. J. Rosseinsky, *Adv. Funct. Mater.*, 2010, **20**, 1599.

16. K. C. Barick, S. Singh, N. V. Jadhav, D. Bahadur, B. N. Pandey and P. A. Hassan, *Adv. Funct. Mater.*, 2012, **22**, 4975.

17. M. Textor, L. Ruiz, R. Hofer, A. Rossi, K. Feldman, G. Hähner and N. D. Spencer, *Langmuir*, 2000, **16**, 3257.

18. C. Yee, G. Kataby, A. Ulman, T. Prozorov, H. White, A. King, M. Rafailovich, J. Sokolov and A. Gedanken, *Langmuir*, 1999, **15**, 7111.

19. O. K. Borggaard, B. Raben-Lange, A. L. Gimsing and B. W. Strobel, *Geoderma*, 2005, **127**, 270.

20. Y. Sahoo. H. Pizem, T. Fried, D. Golodnitsky, L. Burstein, C. N. Sukenik and G. Markovich, *Langmuir*, 2001, **17**, 7907.

21. D. I. Kreller, G. Gibson, W. Novak, G. W. vanLoon and J.H. Horton, *Coll. Surf. A*, 2003, **212**, 249.

22. M. A. White, J. A. Johnson and J. T. Koberstein, *J. Am. Chem. Soc.*, 2006, **128**, 11356.

23. L. Qi, J. Fresnais, P. Muller, O. Theodoly, J. -F. Berret and J. -P. Chapel, *Langmuir*, 2012, **28**, 11448.

24. C. D. Cruz , O. Sandre and V. Cabuil, *J. Phys. Chem. B*, 2005, **109**, 14292.

New Journal of Chemistry Accepted Manuscript

25. G. Lamanna, M. Kueny-Stotz, H. Mamlouk-Chaouachi, C. Ghobril, B. Basly, A. Bertin, I. Miladi, C. Billotey, G. Pourroy, S. Begin-Colin and D. Felder-Flesch, *Biomater.*, 2011, **32**, 8562.

26. J. Auernheimer, D. Zukowski, C. Dahmen, M. Kantlehner, A. Enderle, S. L. Goodman and H. Kessler, *Chem. Bio. Chem.*, 2005, **6**, 2034.

27. H. J. Parab, J. -H. Huang, T. -C. Lai, Y. -H. Jan, R. -S. Liu, J. -L. Wang, M. Hsiao, C. -H. Chen, Y. -K. Hwu, D. P. Tsai, S. -Y. Chuang and J. H. S. Pang, *Nanotechnol.*, 2011, **22**, 395706.

28. A. Gupta, P. Singh and C. Shivakumara, *Sol. State Commun.*, 2010, **150**, 386.

29. N. X. Wang, Y. Q. Wang, X. W. He and W. Y. Li, *J. Nanosci. Nanotechnol.*, 2011, **11**, 4039.

30. M. Kuppayee, G. K. V. Nachiyar and V. Ramasamy, *Appl. Surf. Sci.*, 2011, **257**, 6779.

31. R. Massart, *IEEE Trans. Magn.*, 1981, **MAG-17**, 1247.

32. Y. Sahoo, A. Goodarzi, M. T. Swihart, T. Y. Ohulchanskyy, N. Kaur, E. P. Furlani and P. N. Prasad, *J. Phys. Chem. B*, 2005, **109**, 3879.

33. M. K. Jaiswal, R. Banerjee, P. Pradhan and D. Bahadur, *Coll. Surf. B*, 2010, **81**, 185.

34. M. Lundqvist, J. Stigler, T. Cedervall, T. Berggård, M. B. Flanagan, I. Lynch, G. Elia and K. Dawson, *ACS Nano,* 2011, **5**, 7503.

35. A. Tiwari, S. A. Khan and R. S. Kher, *Adv. Appl. Sci. Res.*, 2011, **2**, 105.

36. M. R. Ahsan, M.A. Uddin and M. G. Mortuza, *Indian J. Pure Appl. Phys.*, 2005, **43**, 89.

37. J. E. Wong, A. K. Gaharwar, D. Müller-Schulte, D. Bahadur and W. Richtering, *J. Nanosci. Nanotechnol.*, 2008, **8**, 4033.

38. R.S. Ningthoujam and N.S. Gajbhiye, *Mater. Res. Bull.,* 2010, **45,** 499.

New Journal of Chemistry Accepted Manuscript

39. R.E. Rosensweig, *J. Magn. Magn. Mater.*, 2002, **252**, 370.

40. R. Hergt and W. Andrä, in *Magnetism in Medicine: A Handbook*, ed. W. Andrä and H. Nowak, Wiley-VCH Verlag GmbH & Co. KGaA, Weinheim, Germany, 2nd edn., 2007, ch. 4.6, pp. 550-570.

41. H. M. Joshi, Y. P. Lin, M. Aslam, P. V. Prasad, E, A. Schultz-Sikma, R. Edelman, T. Meade and V. P. Dravid, *J. Phys. Chem. C*, 2009, **113**, 17761.

42. N. K. Prasad, K. Rathinasamy, D. Panda and D. Bahadur, *J. Mater. Chem.*, 2007, **17**, 5042.

43. J. P. Fortin, C. Wilhelm, J. Servais, C. Menager, J. C. Bacri and F. Gazeau, *J. Am. Chem. Soc.*, 2007, **129**, 2628.

44. E. Munnier, F. Tewes, S. Cohen-Jonathan, C. Linassier, L. Douziech-Eyrolles, H. Marchais, M. Soucé, K. Hervé, P. Dubois and I. Chourpa, *Chem. Pharm. Bull.*, 2007, **55**, 1006.

45. F. A. D. Wolf, K. Nicolay and B. D. Kruijff, *Biochem.*, 1992, **31**, 9252.

46. T. J. Higuchi, *J. Pharm. Sci.*, 1963, **52**, 1145.

47. H. Oliveira, E. Pérez-Andrés, J. Thevenot, O. Sandre, E. Berra and S. Lecommandoux, *J. Control. Release*, 2013, **169**, 165.

New Journal of Chemistry Accepted Manuscript